

Quiet time particle acceleration in interplanetary space

F. Lepreti¹, H. Isliker¹, K. Petraki^{1,2}, and L. Vlahos¹

¹ Department of Physics, Aristotle University of Thessaloniki, 54124 Thessaloniki, Greece
e-mail: lepreti@astro.auth.gr

² Department of Physics and Astronomy, UCLA, Los Angeles, California 90095, USA

Received 16 July 2004 / Accepted 8 November 2004

Abstract. We propose a model for the acceleration of charged particles in interplanetary space that appear during quiet time periods, that is, not associated with solar activity events like intense flares or coronal mass ejections. The interaction of charged particles with modeled turbulent electromagnetic fields, which mimic the fields observed in the interplanetary medium, is studied. The turbulence is modeled by means of a dynamical system, the Gledzer-Ohkitani-Yamada (GOY) shell model, which describes the gross features of the Navier-Stokes equations. The GOY model is used to build a 3D velocity field, which in turn is used to numerically solve the ideal magneto-hydrodynamic (MHD) induction equation, while the electric field is calculated from the ideal Ohm's law. Particle acceleration in such an environment is investigated by test particle simulations, and the resulting energy distributions are discussed and compared to observations of suprathermal electrons and ions during quiet periods in interplanetary space.

Key words. acceleration of particles – turbulence – Sun: solar wind – interplanetary medium

1. Introduction

The observations of high energy, suprathermal particle populations in interplanetary space reveal the presence of a rich variety of physical characteristics and processes (see Reames 1999, for a review). The information recovered from time profiles of particle fluxes, energy spectra, element abundances, ionization states, etc., is essential in determining many properties of the sources and of the mechanisms of particle acceleration. The remarkable heterogeneity found in the detected energetic particle events is related, in large part, to the existence of different sources of acceleration in interplanetary space. Suprathermal populations can be produced by solar flares, collisionless shock waves driven by Coronal Mass Ejections (CMEs), Corotating Interaction Regions (CIRs), or the heliospheric termination shock.

For many years, the attention of researchers has been focused on suprathermal particles with energies above a few hundred keV, due to the fact that the spacecraft instruments lacked the sensitivity needed to investigate the energy range from the solar wind thermal plasma up to a few hundred keV. In recent years, however, with the launch of the Ulysses, Advanced Composition Explorer (ACE), and WIND spacecrafts, this gap has been filled and observations of “quiet time” suprathermal particles, that is, not associated with the abrupt energization events mentioned above, have become available.

The electron spectrum, measured between ~ 5 eV and ~ 100 keV by the 3D Plasma and Energetic Particles Experiment (Lin et al. 1995) on the WIND spacecraft during

a quiet period, has been investigated by Lin (1998). A Maxwellian core dominates the spectrum from ~ 5 eV to ~ 50 eV, while a hotter population, the so-called solar wind halo (Feldman et al. 1975), takes over in the range between ~ 100 eV to ~ 1 keV, due to the escape of coronal thermal electrons with temperature of $\sim 10^6$ K. However, these WIND observations have made possible the identification of a third, much harder component, which has been denoted the “super-halo”, with energies from ~ 2 keV up to ≥ 100 keV and an approximate power law shape with exponent ~ 2.5 . The angular distribution of these “super-halo” electrons is nearly isotropic. According to Lin (1998), this high energy population is not solar in origin, since this would imply a continuous production and escape of electrons with such energies from the Sun. It has been suggested (Lin 1998) that the “super-halo” tail is due to acceleration by CIRs beyond 1 AU, but clear evidence for correlations with CIRs or solar active regions have not yet been found.

The velocity distributions of solar wind ions from 0.6 to 100 keV/e, measured using the Solar Wind Ion Composition Spectrometer (SWICS) instruments on Ulysses and ACE (Gloeckler et al. 1992, 1995), have been studied in Gloeckler (1999), Gloeckler et al. (2000), and Gloeckler (2003). One of the most important findings of these works is that the speed distributions of H^+ , He^+ and He^{++} ions show well developed, approximate power law tails during quiet time periods, that is, far from shocks, CIR compressions and other disturbances. This indicates the presence of a population of highly suprathermal ions at all times. The power law exponents of

these tails, which extend over the whole measurement range, are between ~ 5 and ~ 5.5 in the slow, in-ecliptic solar wind, and ~ 8 in the super-quiet fast wind coming from polar coronal holes. Comparing ACE observations at ~ 1 AU to Ulysses observations at ~ 5 AU, the authors also found that the tails are continuously regenerated in the out-flowing solar wind, overcoming the cooling related to the wind expansion. The main question arising from these observations is how these ubiquitous suprathermal ions are produced in the quiet solar wind when there are no shocks, CIRs or other disturbances observed locally. le Roux et al. (2001) suggested that pickup ions might be accelerated by large-scale turbulent electric fields directed along the background magnetic field. In order to explore this possibility, they presented a numerical model for gyro-tropic, pitch-angle dependent pickup ion transport between the Sun and the Earth based on standard kinetic theory for charged particles. The ion kinetic transport equation used in their model includes a Gaussian random value representation of the large-scale field-aligned electric field fluctuations averaged over the characteristic length and time scales of MHD turbulence in the low-latitude solar wind. The authors choose the standard deviation of these electric fields by requiring the reproduction of observed accelerated pickup ion spectra and in this way they were able to obtain a qualitative agreement of the results of their model with the suprathermal He⁺ spectra in the slow low-latitude solar wind, observed at ~ 1 AU.

Kirsch & Mall (2003) recently presented an analysis of interplanetary suprathermal ions, based on measurements performed with the SMS experiment (Gloeckler et al. 1995) on the WIND spacecraft, in the range 0.5–225 keV/e. The authors investigated particle bursts in which high energy protons in the range 5–100 keV are observed in association with distinct decreases of the magnetic field magnitude. They considered only events not associated with shocks, CIRs, and magnetospheric disturbances. As a consequence of the observed magnetic field behaviour, they suggest that these bursts could be the result of a local reconnection process, or, alternatively, they propose that inductive electric fields (i.e. $\nabla \times \mathbf{E} = -(1/c)\partial\mathbf{B}/\partial t$) could be a possible explanation for the observed particle acceleration.

Here, we investigate with a new approach the possibility that the high energy particles observed in the interplanetary space during quiet time periods are due to a process of stochastic acceleration in the turbulent electromagnetic fields present in the heliospheric plasma. Recently, the stochastic acceleration process in turbulent electromagnetic fields has been investigated with numerical experiments in which test particle simulations are performed in field configurations that are obtained from the solution of the magneto-hydrodynamic (MHD) equations (Nodes et al. 2003; Dmitruk et al. 2003). The authors suggest that these simulations could potentially be applied to astrophysical problems. As an alternative approach, other authors have studied the motion of test particles in electromagnetic fields built up by means of suitable models for particular applications, like the Earth's magnetotail (Veltri et al. 1998) or the solar corona (Arzner & Vlahos 2004). With respect to other approaches, test particle simulations offer the possibility to describe some peculiar features of particle acceleration

in turbulent fields, especially the possibility for particles to be trapped, possibly in or around strong, coherent electric field regions, leading to effective acceleration even for low initial energies (Ambrosiano et al. 1988; Dmitruk et al. 2003).

In the present paper, we present a model for stochastic, quiet time particle acceleration in the interplanetary space, based on turbulent electromagnetic fields constructed by means of the so-called Gledzer-Ohkitani-Yamada (GOY) shell model (Gledzer 1973; Yamada & Ohkitani 1987), which mimics the nonlinear dynamics of fluid turbulence. The use of such a simplified description of turbulence implies that we can describe only some basic features of the nonlinear interactions occurring in turbulent fluids, with the advantage that we can simulate turbulent electromagnetic field configurations without the computational difficulty of solving the full MHD equations. The magnetic field is determined through the MHD induction equation, assuming weak magnetic fields so that the back reaction onto the plasma can be neglected. The electric field is given by Ohm's law. In this framework, we perform test particle simulations, concentrating mainly on the energetics of the injected particles, i.e. electrons and ions.

A basic description of the model is given in Sect. 2. In Sect. 3, we present the numerical simulations performed and the results obtained from them. Discussions and conclusions are given in Sect. 4.

2. The model

The model describes the acceleration of charged test particles in turbulent electromagnetic fields, as obtained from a dynamical system model of turbulence. In general, the macroscopic description of a plasma is given by the magneto-hydrodynamic (MHD) equations (see e.g. Boyd & Sanderson 2003). Here, we consider particle acceleration events occurring in regions of the interplanetary space where the magnetic field is weak, so that we can restrict ourselves to weakly magnetized plasmas, which implies that the temporal evolution of the plasma is governed by the velocity field. In order to build up the velocity field configurations, we use the so-called GOY shell model, through which it is possible to generate a turbulent, incompressible 3D velocity field $\mathbf{V}(\mathbf{r}, t)$, as will be explained in Sect. 2.1.

The velocity field is used to obtain numerical solutions of the MHD induction equation for a perfectly conducting plasma, namely

$$\frac{\partial \mathbf{B}}{\partial t} = \nabla \times (\mathbf{V} \times \mathbf{B}), \quad (1)$$

where \mathbf{B} is the magnetic field. The dissipative term $\mu \nabla^2 \mathbf{B}$ (where μ is the magnetic diffusivity) is not taken into account, since the plasma in the interplanetary space can be considered collisionless to a good approximation (see e.g. Montgomery 1983). The electric field is then computed from the ideal Ohm's law

$$\mathbf{E} = -\frac{1}{c} \mathbf{V} \times \mathbf{B}, \quad (2)$$

where the resistive term $\eta \mathbf{j}$ (with η being the resistivity and \mathbf{j} the current density, respectively) is again neglected. As already

mentioned before, the feedback of the magnetic field on the velocity field (that is, the effect of the Laplace force) is not considered, as the velocity field is given independently and the MHD momentum equation is not considered. In other words, we suppose that the magnetic energy density is much smaller than the kinetic energy density of the turbulent flow.

To investigate the acceleration of test particles in the electromagnetic fields generated as described above, we consider the relativistic equations of motions of a charged particle in an external electromagnetic field:

$$\frac{d\mathbf{r}}{dt} = \mathbf{v} \quad (3)$$

$$\frac{d\mathbf{p}}{dt} = q\mathbf{E} + \frac{q}{c}\mathbf{v} \times \mathbf{B}, \quad (4)$$

where \mathbf{r} , \mathbf{v} , and \mathbf{p} are the position, velocity, and momentum of the particle, respectively, c the speed of light, and q the charge of the particle. For the numerical integration, we express Eq. (4) in terms of velocity ($m\gamma\mathbf{v} = \mathbf{p}$),

$$\frac{d\mathbf{v}}{dt} = \frac{q}{\gamma m}\mathbf{E} + \frac{q}{\gamma mc}\mathbf{v} \times \mathbf{B} - \frac{q}{\gamma mc^2}\mathbf{v}(\mathbf{v} \cdot \mathbf{E}), \quad (5)$$

where $\gamma = 1/\sqrt{1-v^2/c^2}$, and m is the mass of the particle.

2.1. Construction of the 3D fluid velocity field

The 3D, time-dependent velocity field $\mathbf{V}(\mathbf{r}, t)$ is constructed by means of the so-called GOY shell model for turbulence. Shell models (see Bohr et al. 2000, for a complete review) are dynamical systems designed to represent in a simplified way the spectral form of the equations which describe turbulent fluids. They were originally proposed by Obukhov (1971), Desnyansky & Novikov (1974), and Gledzer (1973) for hydrodynamic turbulence. The GOY shell model (Gledzer 1973; Yamada & Ohkitani 1987) has been extensively investigated, both analytically and numerically (Yamada & Ohkitani 1987; Jensen et al. 1991; Biferale et al. 1995). In the following, we describe some basic characteristics of the GOY model.

The main idea of the GOY shell model is to mimic the Navier-Stokes equations by a dynamical system in which the velocity field fluctuations at different length scales are represented by scalar variables $u_n(t)$. To this aim, the Fourier space is divided into N shells, with the associated wave number denoted by k_n , where the shell index n is discrete. The scalar, complex variable $u_n(t)$ is associated with the n th shell, and the nonlinear dynamics of turbulent fluids are modeled by quadratic couplings among nearest and next nearest neighbour shells, following the assumption that the nonlinear interactions are local in the k space. The coefficients of the nonlinear terms are determined by imposing the conservation of the ideal invariants of the Navier-Stokes equations. The equations of evolution of the dynamical variables $u_n(t)$ are (Bohr et al. 2000)

$$\left(\frac{d}{dt} + \nu k_n^2\right)u_n = i\left(\alpha k_{n+1}u_{n+2}^*u_{n+1}^* + \beta k_n u_{n+1}^*u_{n-1}^* + \gamma k_{n-1}u_{n-1}^*u_{n-2}^*\right) + \delta_{mn}f_n, \quad (6)$$

where $n = 1, \dots, N$.

The parameter ν stands for the kinematic viscosity, while $\delta_{mn}f_n$ is a stochastic forcing term acting on the shell m , one of the first shells, providing a constant average energy flux into the system (δ_{mn} is the Kronecker symbol). The wave numbers are chosen to follow the relation

$$k_n = k_0 h^n, \quad (7)$$

where k_0 and h are constant ($h > 1$, usually $h = 2$), and $n > 1$. The shells are thus equally spaced in a logarithmic scale, which is justified by the fact that in fully developed turbulence the energy spectrum in the nonlinear, inertial range follows a power law.

One of the main advantages of shell models over numerical simulations of the Navier-Stokes equations is that they can be investigated at much higher Reynolds numbers. They provide a good description of the scaling properties of fully developed turbulence in the inertial range, even if, being scalar models, they do not include information about the spatial structures of turbulence. From the scalar variables $u_n(t)$ we can generate an incompressible velocity field $\mathbf{V}(\mathbf{r}, t)$ in the real 3D space by applying a simple numerical algorithm (Bohr et al. 2000). The dynamical variables $u_n(t)$ of the shell model are supposed to represent the coefficients of a Fourier expansion with wave vectors \mathbf{k} in a shell of radius $|\mathbf{k}| = k_n$. We introduce a set of vectors \mathbf{k}_n :

$$\mathbf{k}_n = k_n \mathbf{e}_n, \quad (8)$$

where $\mathbf{e}_n = \{e_n^{(1)}, e_n^{(2)}, e_n^{(3)}\}$ are randomly chosen vectors of unit norm. The components $V_j(\mathbf{x}, t)$, $j = 1, 2, 3$, of the velocity field are obtained by the analogue to an inverse Fourier transform,

$$V_j(\mathbf{r}, t) = \sum_{n=1}^N C_n^{(j)} \left[u_n(t) e^{i\mathbf{k}_n \cdot \mathbf{r}} + c.c. \right], \quad (9)$$

where the coefficients $C_n^{(j)}$ are of order $O(1)$.

In order to satisfy the incompressibility constraint $\nabla \cdot \mathbf{V} = 0$, the vectors $\mathbf{e}_n = \{e_n^{(1)}, e_n^{(2)}, e_n^{(3)}\}$ and the coefficients $C_n^{(j)}$ must satisfy the condition

$$\sum_{j=1}^3 C_n^{(j)} e_n^{(j)} = 0, \quad \forall n. \quad (10)$$

3. Numerical simulations and results

The numerical investigation consists of two main steps: 1) the calculation of the magnetic and electric fields from Eqs. (1) and (2), in which the velocity field given by Eq. (9) is used; 2) test particle simulations through the numerical solutions of Eqs. (3) and (5).

3.1. Magnetic and electric field calculation

The GOY shell model equations Eq. (6) are solved by using a 4th order Runge-Kutta integration algorithm, using $N = 22$ shells. The kinematic viscosity in the shell model is assumed to be $\nu = 10^{-7}$. Once the shell model has reached a statistically stationary state, we start the numerical integration

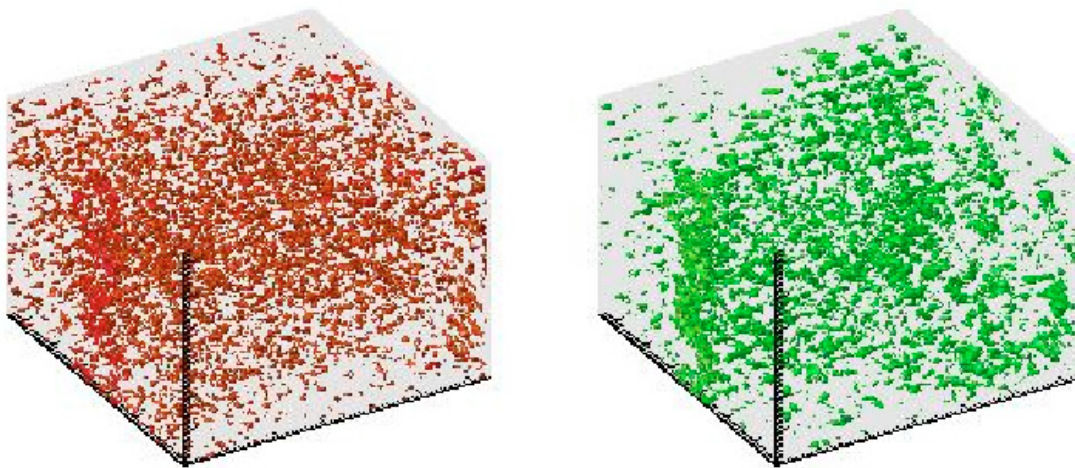


Fig. 1. 3D visualization of the magnetic field intensity $|\mathbf{B}|$ above the threshold $B_{\text{th}} = 1.2 \times 10^{-4}$ G (left panel) and of the electric field intensity $|\mathbf{E}|$ above the threshold $E_{\text{th}} = 1.2 \times 10^{-7}$ statvolt cm^{-1} (right panel).

of the MHD induction equation (Eq. (1)), by using the Wilson upwind scheme (Hawley et al. 1984), imposing free outflow boundary conditions and using the velocity field $\mathbf{V}(\mathbf{r}, t)$ from Eq. (9). The initial magnetic field $\mathbf{B}_0(\mathbf{r})$ is given by a random perturbation constructed through a sum of Fourier modes $\mathbf{B}_0(\mathbf{r}) = \sum_{\mathbf{k}} \mathbf{B}_0(\mathbf{k}) \cos(\mathbf{k} \cdot \mathbf{r} + \varphi_{\mathbf{k}})$, with Gaussian distributed amplitudes $|\mathbf{B}_0(\mathbf{k})|$, random phases $\varphi_{\mathbf{k}}$ and with the constraint $\mathbf{k} \cdot \mathbf{B}_0(\mathbf{k}) = 0$ imposed, as it follows from $\nabla \cdot \mathbf{B} = 0$. The size of the grid is 64^3 . The evolution of the system is followed over a time interval $2\tau_e$, where τ_e is a typical eddy turnover time, given by $\tau_e = L/V_{\text{rms}}$, L being the size of the simulation domain and V_{rms} the rms velocity. The condition that the kinetic energy density is much smaller than the magnetic energy density is checked during the time evolution. We also monitor the value of $\nabla \cdot \mathbf{B}$, evaluated through a standard finite differences scheme, and verify that it does not vary significantly with respect to the initial value, which can be considered zero within the numerical error.

The equations are solved in non-dimensional form, and suitable rescaling factors are applied to describe quiet time periods in interplanetary space. The applied forcing term leads to an rms velocity field intensity of $V_{\text{rms}} \approx 3.2 \times 10^7$ cm s^{-1} . This value is slightly larger than the rms velocity estimates obtained from a 30 year dataset of solar wind observations, which gave values around 7×10^6 cm s^{-1} (Breech et al. 2003). This means that in our simulations we are assuming a slightly enhanced turbulence level with respect to the average. The linear size of the simulation box is assumed to be $L = 2.2 \times 10^{10}$ cm. The rms value of the magnetic field intensity, after the rescaling, is $B_{\text{rms}} \approx 7.4 \times 10^{-5}$ G, while the rescaled rms value of the electric field intensity is $E_{\text{rms}} \approx 5.7 \times 10^{-8}$ statvolt cm^{-1} . These values are slightly larger than the rms values obtained from long time datasets of solar wind observations.

To illustrate the 3D structure of the magnetic and electric fields, in Fig. 1 we present a 3D visualization of the regions where the magnetic field and electric field intensities exceed the thresholds $B_{\text{th}} = 1.2 \times 10^{-4}$ G and $E_{\text{th}} = 1.2 \times 10^{-7}$ statvolt cm^{-1} , respectively.

In Fig. 2 we present the Probability Density Functions (PDFs) of the three electric field components, collected at a fixed time from the entire simulation box. In order to compare the different PDFs, the variables are first translated to zero mean and then normalized to their standard deviation, so that all the PDFs have zero mean and unit standard deviation. As it can be seen, these PDFs are not Gaussian, they exhibit clear exponential tails. This result is in qualitative agreement with the one-point PDFs of the observed interplanetary induced electric fields (IEF) presented in Breech et al. (2003). In a more recent work (Sorriso-Valvo et al. 2004), it has been shown that the statistical properties of the IEF depend on the wind velocity, an effect that we do not model here (see discussion in Sect. 4).

3.2. Test particle simulations

In this subsection, we present some results obtained from test particle simulations of electrons and ions in the electromagnetic field configurations generated as described in the previous subsection. Specifically, the magnetic and electric field configurations obtained at the time $2\tau_e$ during the evolution of Eq. (1) are used. The particle motion Eqs. (3) and (5) are solved with a 4th order Runge-Kutta, adaptive step-size scheme. The magnetic and electric field configurations are kept constant during the time we monitor the particles, assuming a much slower evolution time for the fluid velocity field than for the test particles. Since the magnetic and the electric fields are given only at a discrete set of points, both fields are interpolated with a local, 3D linear interpolation to provide the field values in between grid-points, wherever they are needed for the integration scheme. The initial time step used for the integration is set to $0.1t_g$, where t_g is the gyration period of the particles at the starting point.

The charged test particles are injected at random positions within the simulation box, with velocities extracted from the tail of a Maxwellian distribution with temperature $T = 1.15 \times 10^5$ K (corresponding to ~ 10 eV), which represents a typical value in the interplanetary space at 1 AU from the Sun. The threshold velocity used to select only the particles in the tail of

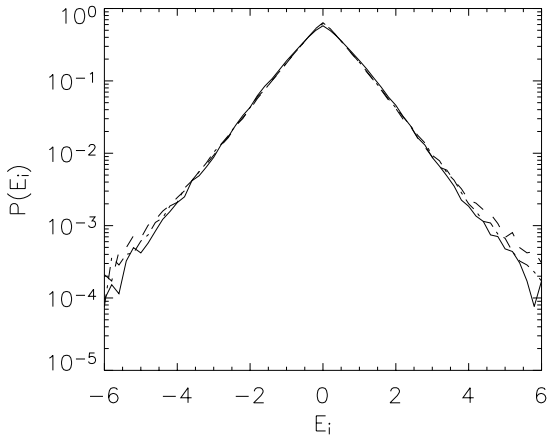


Fig. 2. PDFs of the three components of the electric field: the solid, dashed, and dot-dashed lines represent the PDFs of E_x , E_y , and E_z respectively.

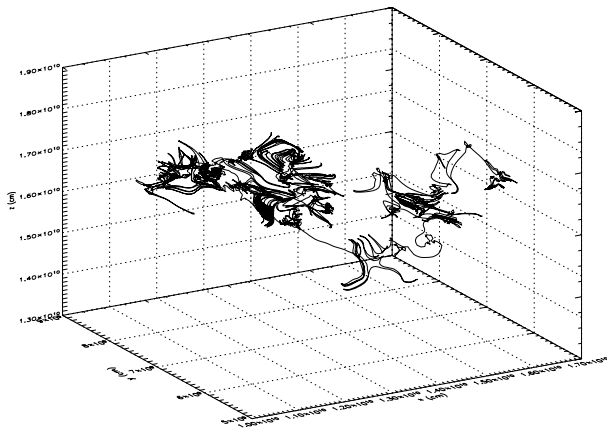


Fig. 3. Trajectory of a test electron.

the Maxwellian is $2v_{th}$, where v_{th} is the thermal velocity. The choice to use only the tail of the initial Maxwellian distribution is due to the fact that we do not model the collisional processes occurring in the interplanetary space plasma, so we assume that only the high energy part of the distribution participates in the acceleration process. If a particle leaves the simulation box before the end of its tracing time interval, it is reinjected into the box at a random point on the surface opposite to the one through which it had left. The maximum tracing time interval used in this work is $t = 300$ s, which is much smaller than the typical collision times for electrons and ions with velocities larger than twice the thermal velocity (see e.g. Montgomery 1983), so that we can neglect collisional effects.

In Fig. 3, a sample trajectory of a typical test electron is shown. It can be seen that, during its irregular motion, the particle visits both regions where it remains trapped for some time and regions where its motion exhibits long “jumps”, as could be expected in a turbulent field environment. In Fig. 4, we report part of the time evolution of the kinetic energy of a typical test electron (upper panel), the associated electric field intensity along the trajectory (middle panel), and the cosine of the angle α between the particle velocity and the electric field (lower panel).

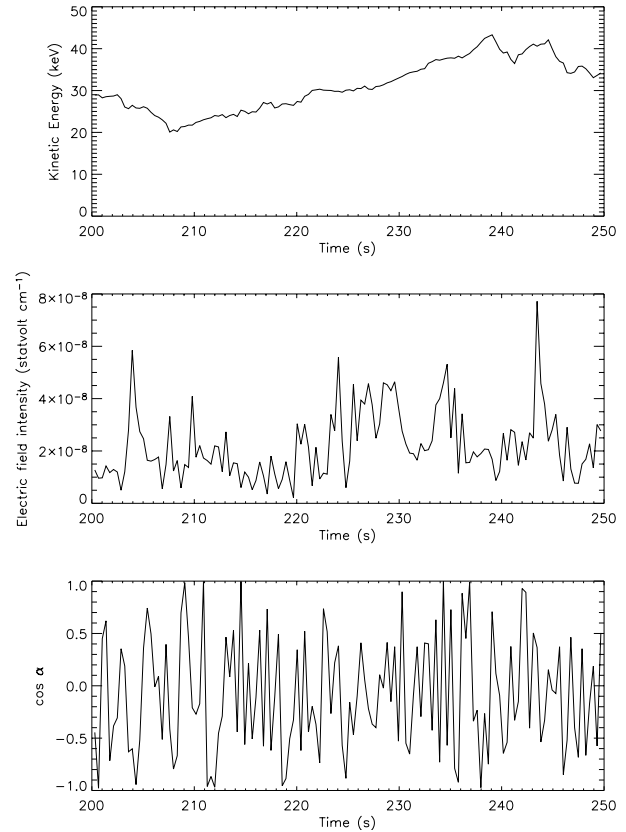


Fig. 4. Part of the time evolution of the kinetic energy of a test electron (upper panel), the associated electric field intensity along the trajectory (middle panel), and the cosine of the angle α between the particle velocity and the electric field (lower panel).

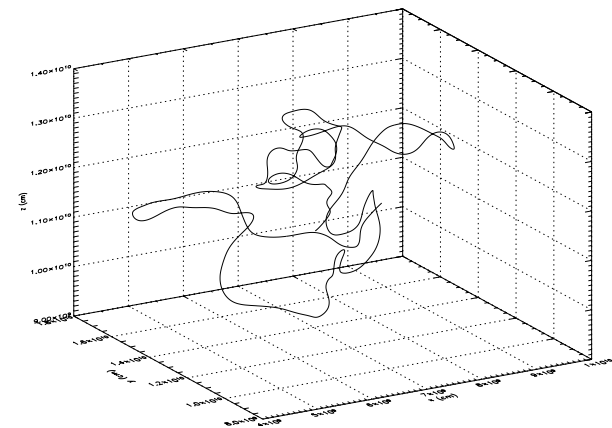


Fig. 5. Trajectory of a test proton.

In Fig. 5, a sample trajectory of a test proton is shown. As is expected, the typical shape of the proton trajectories is substantially different from the one of the electrons, due to the much larger mass of the protons. In Fig. 6, we report part of the time evolution of the kinetic energy of a test proton (upper panel), the associated electric field intensity along the trajectory (middle panel), and the cosine of the angle α between the particle velocity and the electric field (lower panel). From this figure, it is more clear, with respect to the figure referring to electrons (Fig. 4), that the largest kinetic energy variations are

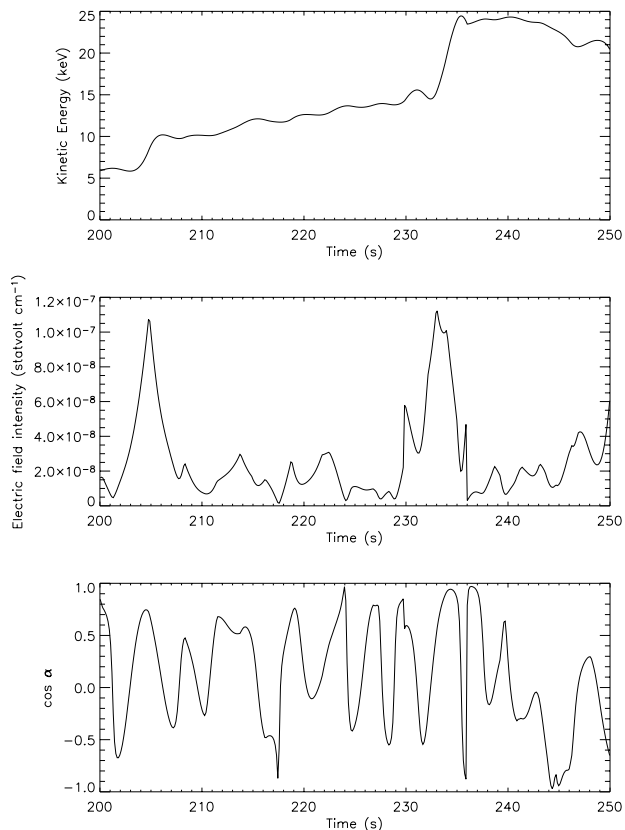


Fig. 6. Part of the time evolution of the kinetic energy of a test proton (*upper panel*), the associated electric field intensity along the trajectory (*middle panel*), and the cosine of the angle α between the particle velocity and the electric field (*lower panel*).

associated both with intense electric field spikes and with extended regions of almost coalignment between particle velocity and electric field.

In Fig. 7, we report the kinetic energy PDFs of 10^4 test electrons at the initial time $t = 0$ s, and at three successive times $t = 1$ s, $t = 30$ s, and $t = 300$ s respectively. At $t = 1$ s, the evolution of the initial Maxwellian distribution produces a tail, extending to ~ 5 keV, which does not show a clear, unique power law form, but is more of a double power-law shape. As the time increases, the high energy tail tends to become exponential with maximum energy up to ~ 100 keV

In Fig. 8, we report the kinetic energy PDFs of 10^4 test protons at the same times as for the electrons. The evolution of the proton distributions is qualitatively similar to the electrons', although the PDF tail at $t = 1$ s now displays a reasonably clear power law scaling that persists until 30 s. However, for $t = 300$ s the tail is narrow and steep, reminiscent of both a steep power-law and an exponential distribution, with maximum energy up to ~ 100 keV.

Since observations are also available for other ions, and in particular for He ions, we also investigated the kinetic energy PDF of He⁺ ions. The time evolution of this PDF, shown in Fig. 9, is quite similar to the proton case. For $t = 1$ s, the tail of the PDF extends to lower energies than for the protons, again being a power-law shape that persists until $t = 30$ s.

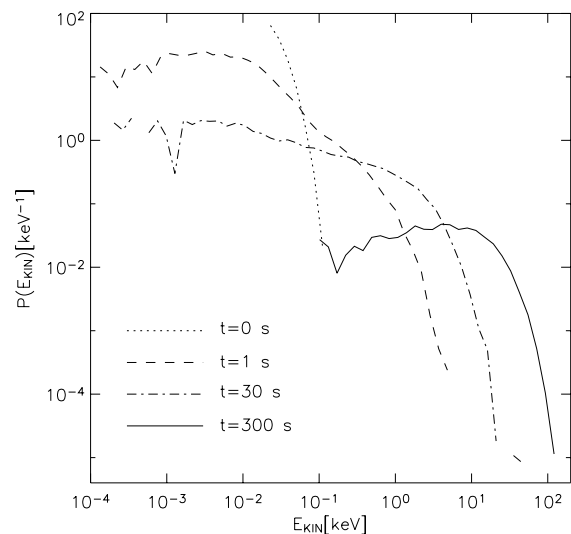


Fig. 7. Kinetic energy probability density function of 10^4 test electrons at the initial time $t = 0$ (dotted curve), and after $t = 1$ s (dashed curve), $t = 30$ s (dot-dashed curve), $t = 300$ s (solid curve).

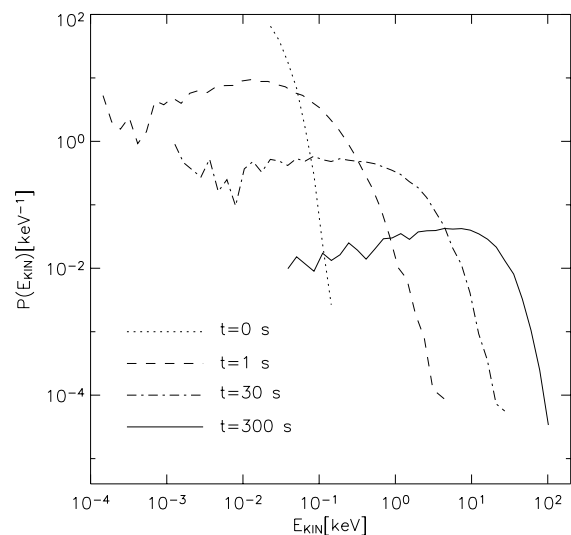


Fig. 8. Kinetic energy probability density function of 10^4 test protons at the initial time $t = 0$ (dotted curve), and after $t = 1$ s (dashed curve), $t = 30$ s (dot-dashed curve), $t = 300$ s (solid curve).

For $t = 300$ s, energies up to ~ 100 keV are reached, with a narrow and steep tail that is difficult to classify.

4. Discussion and conclusion

In this paper, we have presented a model for turbulent particle acceleration based on a dynamical system description of turbulence. The aim of the model is to describe long lasting particle acceleration processes occurring in the turbulent interplanetary space during quiet time periods, which lead to the appearance of suprathermal tails at all times in the energy distributions of electrons and ions (extending up to ~ 100 keV).

The acceleration process has been investigated by performing test particle numerical simulations in the electromagnetic

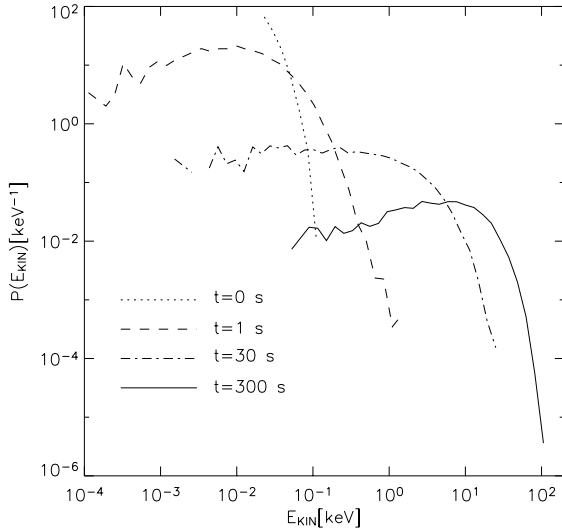


Fig. 9. Kinetic energy probability density function of 10^4 test He^+ ions at the initial time $t = 0$ (dotted curve), and after $t = 1$ s (dashed curve), $t = 30$ s (dot-dashed curve), $t = 300$ s (solid curve).

fields obtained by numerically solving the ideal MHD induction equation, which is driven by the velocity field that is calculated using a dynamical system model (the so-called GOY shell model) of turbulence. This approach implies that the magnetic fields are supposed to be weak, or that the magnetic energy density is much smaller than the kinetic energy density of the flow.

The PDFs of the electric field components have been shown to be non-Gaussian, exhibiting exponential tails. The presence of roughly exponential tails in the one-point PDFs of the interplanetary induced electric fields (IEF) has been recently shown based on data analysis performed on 30 years of measurements that were acquired by different spacecrafts (Breech et al. 2003). However, more recently (Sorriso-Valvo et al. 2004), it has been shown that using homogeneous datasets with respect to wind velocity and solar activity, that is, considering short datasets and separating the data according to slow and fast wind streams, the exponential tails are recovered only in the radial components of the electric field, that is, the component along the Sun-Earth direction, which coincides with the mean wind direction. Our model is obviously not able to reproduce in detail these statistical properties of the observed IEF, since we do not take into account some basic features of the solar wind structure, e.g. its mean bulk velocity, mean magnetic field structure, etc. In other words, we consider only the effect of field fluctuations related to the presence of turbulence.

With our approach, we have been able to obtain basic physical insights into the process of particle acceleration due to turbulent electric fields in weakly magnetized plasmas, and to investigate the possibility that this mechanism plays a role in the acceleration of charged particles to suprathermal energies in interplanetary space during quiet periods. The trajectories obtained from the simulations indicate that the particles alternately visit regions in which they are trapped for some time, due to the effects of turbulence, and other regions where long “jumps” are observed. The observed motion of the test

particles suggests that a Fokker-Planck description of the diffusion process underlying the particle acceleration is not sufficient to achieve a complete characterization of the problem. This is one of the main reasons why a test particle approach is adequate in studying such situations.

We found that, starting from an initial thermal population, both in the case of electrons and ions, the initial Maxwellian energy distributions evolve in time, giving rise to power-law tails for shorter times, which become very steep and narrow for the longest time we monitor the particles, so that it is difficult to discriminate between exponential and power-law distributions. At the maximum time we allow, the particles reach energies up to ~ 100 keV. The fact that our model is able to reproduce the observed energies suggests that a stochastic acceleration mechanism resulting from the turbulence that is developed in the interplanetary space can be at the origin of the ubiquitous suprathermal tails observed during quiet time periods, even if the detailed shape of the observed distributions, which exhibit approximate power law tails, is not very well recovered by our model.

The difficulty in reproducing the observations in detail at this stage is related to some limitations of our model in its current form. Our main simplifying assumptions are: (1) We have assumed that the magnetic energy density is much smaller than the kinetic energy density of the fluid. This assumption is often not fulfilled in the interplanetary space, due to the presence of a strong Alfvénic component in the solar wind turbulence (see e.g. Goldstein et al. 1995; Tu & Marsch 1995). (2) The detailed properties of intermittency in solar wind turbulence (see e.g. Burlaga 1991, 1992; Marsch & Liu 1993; Carbone et al. 1995) are not included in the model, and this could have an effect especially on the high energy part of the kinetic energy PDFs. (3) The resistivity, which modifies the small-scale structure of the electric field, is treated as a constant, not taking its possible dynamic evolution into account (see Dmitruk et al. 2003; Arzner & Vlahos 2004). (4) The large scale magnetic field structure, which was not included in the present study, but which nevertheless would be interesting to be investigated, will have a less deciding influence on the energetics.

In order to overcome the limitation (1), a dynamical system for MHD turbulence must be considered, instead of a hydrodynamical model, whereas for the limitation (2), a more appropriate description of intermittency should be introduced in the reconstruction of the 3D fields from the 1D scalar fields that are yielded by the shell models. The presented results suggest that on modifying our model in this way, better compatibility with the observations can be reached.

Acknowledgements. This work was partially supported by the Research Training Network (RTN) “Theory, Observation, and Simulation of Turbulence in Space Plasmas”, funded by the European Commission (contract No. HPRN-CT-2001-00310).

References

Ambrosiano, J., Matthaeus, W. H., Goldstein, M. L., & Plante, D. 1988, *J. Geophys. Res.*, 93, 14383

- Arzner, K., & Vlahos, L. 2004, *ApJ*, 605, L69
- Biferale, L., Lambert, A., Lima, R., & Paladin, G. 1995, *Physica D*, 80, 105
- Bohr, T., Jensen, M. H., Paladin, G., & Vulpiani, A. 2000, *Dynamical Systems Approach to Turbulence* (Cambridge: Cambridge University Press)
- Boyd, T. M. J., & Sanderson, J. J. 2003, *The Physics of Plasmas* (Cambridge: Cambridge University Press)
- Breech, B., Matthaeus, W. H., Milano, L., & Smith, C. W. 2003, *J. Geophys. Res.*, 108, 10.1029/2002JA009529
- Burlaga, L. 1991, *J. Geophys. Res.*, 96, 5847
- Burlaga, L. 1991, *J. Geophys. Res.*, 97, 4283
- Carbone, V., Veltri, P., & Bruno, R. 1995, *Phys. Rev. Lett.*, 75, 3110
- Desnyansky, V. N., & Novikov, E. A. 1974, *Atmos. Oceanic Phys.*, 10, 127
- Dmitruk, P., Matthaeus, W. H., Seenu, N., & Brown, M. R. 2003, *ApJ*, 597, L81
- Feldman, W. C., Asbridge, J. R., Bame, S. J., Montgomery, M. D., & Gary, S. P. 1975, *J. Geophys. Res.*, 80, 4181
- Gledzer, E. B. 1973, *Sov. Phys. Dokl.*, 18, 216
- Gloeckler, G. 1999, *Space Sci. Rev.*, 89, 91
- Gloeckler, G. 2003, in *Solar Wind Ten: Proceedings of the Tenth International Solar Wind Conference*, ed. M. Velli, R. Bruno, & F. Malara, *AIP Conf. Proc.*, 679, 577
- Gloeckler, G., Geiss, J., Balsiger, H., et al. 1992, *A&AS*, 92, 267
- Gloeckler, G., Balsiger, H., Bürgi, A., et al. 1995, *Space Sci. Rev.*, 71, 79
- Gloeckler, G., Fisk, L. A., Zurbuchen, T. H., & Schwadron, N. A. 2000, in *Acceleration and Transport of Energetic Particles Observed in the Heliosphere*, ed. R. A. Mewaldt et al., *AIP Conf. Proc.*, 528, 221
- Goldstein, M. L., Roberts, D. A., & Matthaeus, W. H. 1995, *ARA&A*, 33, 283
- Hawley, J. F., Smarr, L. L., & Wilson, J. R. 1984, *ApJ*, 55, 211
- Jensen, M. H., Paladin, G., & Vulpiani, A. 1991, *Phys. Rev. A*, 43, 798
- Kirsch, E., & Mall, U. 2003, *A&A*, 400, 729
- le Roux, J. A., Matthaeus, W. H., & Zank, G. P. 2001, *Geophys. Res. Lett.*, 28, 3831
- Lin, R. P. 1998, *Space Sci. Rev.*, 86, 61
- Lin, R. P., Anderson, K. A., Ashford, S., et al. 1995, *Space Sci. Rev.*, 71, 125
- Marsch, E., & Liu, S. 1993, *Ann. Geophys.*, 11, 227
- Montgomery, D. 1983, in *Solar Wind Five*, *NASA Conf. Publ.*, CP-2280, 107
- Nodes, C., Birk, G. T., Lesch, H., & Schopper, R. 2003, *Phys. Plasmas*, 10, 835
- Obukhov, A. M. 1971, *Atmos. Oceanic Phys.*, 7, 41
- Reames, D. V. 1999, *Space Sci. Rev.*, 90, 413
- Sorriso-Valvo, L., Carbone, V., & Bruno, R. 2004, *Europhys. Lett.*, 67, 504
- Tu, C.-Y., & Marsch, E. 1995, *Space Sci. Rev.*, 73, 1
- Veltri, P., Zimbardo, G., Taktakishvili, A. L., & Zelenyi, L. M. 1998, *J. Geophys. Res.*, 103, 14897
- Yamada, M., & Ohkitani, K. 1987, *J. Phys. Soc. Jpn*, 56, 4810